Applied Catalysis B: Environmental 198 (2016) 493–507

Contents lists available at ScienceDirect

Applied Catalysis B: Environmental

journal homepage: www.elsevier.com/locate/apcatb

# One-pot synthesis of ordered mesoporous NiMo-$Al_2O_3$ catalysts for dibenzothiophene hydrodesulfurization

Huan Liu[a,b], Yanpeng Li[a], Changlong Yin[a,**], Yilan Wu[a], Yongming Chai[a], Daoming Dong[a], Xuehui Li[a], Chenguang Liu[a,*]

[a] State Key Laboratory of Heavy Oil Processing and Key Laboratory of Catalysis of CNPC, China University of Petroleum, Qingdao 266580, PR China
[b] State Key Laboratory of Safety and Control for Chemicals, Sinopec Safety Engineering Institute, Qingdao 266071, PR China

ARTICLE INFO

*Article history:*
Received 3 February 2016
Received in revised form 1 June 2016
Accepted 2 June 2016
Available online 3 June 2016

*Keywords:*
Ordered mesopore
One-pot synthesis
Hydrodesulfurization
Ni-Mo-Al catalyst
Dibenzothiophene

ABSTRACT

Ordered mesoporous NiMo-$Al_2O_3$ catalysts with 20.0 wt.% $MoO_3$ and various NiO contents were synthesized by a facile one-pot evaporation-induced self-assembly (EISA) method, using P123 as structure-directing agent and anhydrous ethanol as solvent. The hydrophilic Al-, Ni-, and Mo-containing compounds surrounded the P123 micelles to form a hexagonal mesoporous structure. The NiMo-$Al_2O_3$ catalysts were characterized by a series of techniques, including $N_2$ adsorption, XRD, XRF, TEM, SEM, FT-IR, TG-DSC (for the as-synthesized NiMo-$Al_2O_3$ precursors), and TPR. The catalytic activities were tested in hydrodesulfurization (HDS) of dibenzothiophene (DBT). Results show that calcination at 500 °C can fully remove the surfactant and solvent to form amorphous walls. Molybdenum and nickel atoms were incorporated into the channels of the ordered mesoporous alumina and highly dispersed, maintaining the hexagonal symmetry mesostructures. Incorporations of Ni promoted a transformation of molybdate from tetrahedral to octahedral sites and changed the relative intensities of the TPR peaks. Catalytic results reveal that the ordered mesoporous NiMo-$Al_2O_3$ catalysts had high activities towards DBT. Biphenyl was the abundant product in HDS reactions, and direct desulfurization was the dominant route. A high HDS activity was observed with a Ni/Mo molar ratio of 1:1, which was attributed to more easily reducible molybdate and better dispersion of the $MoS_2$ nanoparticles. The ordered mesoporous NiMo-$Al_2O_3$ catalysts, synthesized by this facile one-pot EISA method, provide a new alternative for industrial HDS process.



## 1. Introduction

Increasing emphasis on the stringent environmental legislations of fossil fuels forces refineries to reduce the sulfur content to an ultra-low level, which nowadays requires no more than 10 μg/g [1–3]. So far, hydrotreating (HDT) is the widely used technology for the removal of heteroatoms (S, N, and metal) from diesel, and in this process the heteroatom-containing compounds react with hydrogen on the catalyst surface under high temperature and pressure, thus to eliminate heteroatoms. Traditional HDS catalysts are composed of active components molybdenum or tungsten sulfides promoted by nickel or cobalt sulfides, and supported on alumina. However, these catalysts encounter with a challenging task when producing the ultra-low sulfur diesel due to low activities. In order to achieve this tough challenge preparations of novel HDS catalysts with enhanced activities are demanded. Several strategies have been proposed for designing highly-active HDS catalysts. Replacements of traditional transition metal sulfur catalysts by noble metal catalysts [1,2], implementations of highly-loaded or unsupported catalysts [4–7], and incorporations of new active phases [4,8,9], show potential industrial applications for the production of ultra-low sulfur diesel. However, several distinct disadvantages of these strategies, like high costs of catalysts, stabilities in severe reaction conditions (high temperature and pressure), and resistances to the sulfur poisoning, still remain to be solved [1,2].

Apart from the above strategies applications of functional catalyst supports provide alternatives for the preparations of novel HDS catalysts. Breysse et al. [10] and Dhar et al. [11] reviewed the effects of several supports, including alumina, titania, zirconia (or mixtures of these oxides), zeolites, carbon, and clays, on the catalytic performances in HDS reactions. Different supports possess diverse textural properties (surface areas, pore volumes, and pore size distributions) and acidities, thus leading to different metal-support

* Corresponding author.
** Corresponding author.
*E-mail addresses:* yincl@upc.edu.cn (C. Yin), cgliu@upc.edu.cn (C. Liu).

http://dx.doi.org/10.1016/j.apcatb.2016.06.004
0926-3373/

interactions. These properties affect the dispersion of active components onto the surfaces of various supports, which are mainly accounted for the different catalytic activities.

Another group of novel supports are mesoporous materials [1,2,12–15], especially the mesoporous alumina [16]. Alumina is widely used in HDS process due to its high surface area, high thermal-stability, and low prices [17]. However, the wide pore size distributions are not salutary for efficient catalytic reactions [16]. Yuan et al. proposed a simple and facile route for the synthesis of ordered mesoporous alumina with a large surface area, narrow pore size distribution, and high thermal stability [18]. Using non-ionic tri-block polymer P123 as structure-directing agent (SDA) and anhydrous ethanol as solvent, ordered mesoporous alumina with tunable pore sizes were successfully synthesized by a solvent evaporation-induced self-assembly (EISA) method [18]. Further incorporations of different metal oxides (NiO, $V_2O_5$, $CeO_2$, and CaO) into the channels of the ordered mesoporous alumina led to novel catalysts with high catalytic activities in various reactions [17,19–21]. Herein, we developed this one-pot EISA method to synthesize NiMo-$Al_2O_3$ catalysts. A series of the ordered mesoporous NiMo-$Al_2O_3$ catalysts were synthesized with 20 wt.% $MoO_3$ and various contents of NiO. To date, there are no reports about the one-pot synthesis of the ordered mesoporous NiMo-$Al_2O_3$ catalysts for HDS reactions. In order to correlate the physicochemical properties with catalytic performances, the ordered mesoporous NiMo-$Al_2O_3$ catalysts were characterized by several techniques, and their catalytic activities were evaluated in HDS of dibenzothiophene (DBT).

## 2. Experimental

### 2.1. Preparation

All reagents (Grade AR) were purchased without any further purification. Nickel nitrate ($Ni(NO_3)_2{\cdot}6H_2O$), ammonium heptamolybdate ($(NH_4)_6Mo_7O_{24}{\cdot}4H_2O$), aluminum isopropoxide ($Al(OPr^i)_3$), 67 wt.% nitric acid ($HNO_3$), and anhydrous ethanol ($C_2H_5OH$) were provided by Sinopharm Chemical Reagent Company (P.R. China) and used for the synthesis of the NiMo-$Al_2O_3$ catalysts. A tri-block copolymer (Pluronic P123, average Mn = 5800, $PEO_{20}PPO_{70}PEO_{20}$, EO = ethylene oxide, and PO = propylene oxide) was purchased from Sigma-Aldrich Company (product of BASF, Germany) served as SDA. DBT ($C_{12}H_8S$) and petroleum ether (boiling range from 90 to 120 °C) were used for catalytic reactions.

By carefully modifying and optimizing the volatilization process, the ordered mesoporous NiMo-$Al_2O_3$ catalysts were synthesized by an improved EISA method [18,19,22,23]. Synthesis of a NiMo-$Al_2O_3$ catalyst with NiO and $MoO_3$ contents of 10.0 and 20.0 wt.%, respectively, was used as a typical example. 2.1 g P123 was first dissolved into 40.0 mL of anhydrous ethanol in a glass beaker (100 mL) at room temperature, and 3.2 mL 67 wt.% $HNO_3$, 4.08 g $Al(OPr^i)_3$, 0.358 g $(NH_4)_6Mo_7O_{24}{\cdot}4H_2O$, and 0.565 g $Ni(NO_3)_2{\cdot}6H_2O$ were successively added to the glass beaker under vigorous stirring. The glass beaker was then covered with a polyethylene film and stirred at room temperature for at least 6 h and then transferred to a 60 °C drying oven to undergo ethanol evaporation. After aging for about 2 days the obtained product became a green foam-like solid (light-yellow and white foam-like solids for pure $Al_2O_3$ and MoAl samples, respectively) [18,19]. The solid product was calcined at 500 °C for 4 h in a static air atmosphere with a ramping temperature of 1 °C $min^{-1}$ to obtain the desired material. As for the synthesis of the other NiMo-$Al_2O_3$ catalysts, the content of $MoO_3$ was always fixed at 20.0 wt.%, while various contents of NiO were added, from 2.5, 5.0, 7.5, 12.5, and 15.0 wt.%. Incorporations of nickel nitrate in the synthesis procedure led to green solids. The obtained NiMo-$Al_2O_3$ catalysts were labeled based on the additives and amounts of NiO in the synthesis procedure, and detailed information about the dominations are reported in Table 1.

Two reference catalysts were prepared by an incipient wetness impregnation method, and the ordered mesoporous alumina and an industrial γ-alumina (BET surface area 277 $m^2\,g^{-1}$ and pore volume 0.54 $cm^3\,g^{-1}$) were used as supports. These two supports were first impregnated by a solution containing desired amount of $Ni(NO_3)_2{\cdot}6H_2O$, and then impregnated by a solution of $(NH_4)_6Mo_7O_{24}{\cdot}4H_2O$ to obtain the NiO and $MoO_3$ loadings of 10 and 20 wt.%, respectively. After each impregnation step the samples were first dried at 80 °C for 12 h and then calcined at 500 °C for 4 h in a static air atmosphere. According to the supports these two catalysts were named NiMo/γ-$Al_2O_3$ and NiMo/meso-$Al_2O_3$ catalysts.

### 2.2. Characterization

The ordered mesoporous NiMo-$Al_2O_3$ catalysts were characterized by a series of techniques, including X-ray diffraction (XRD, X'Pert Pro MPD), $N_2$ adsorption (ChemBET 3000), Fourier-transform infrared (FT-IR, Nicolet), temperature-programmed reduction (TPR, RS232), and transmission electron microscopy (TEM, JEM-2100). Detailed characterization information can be found in our previous papers [4,8].

Combined thermogravimetry and differential scanning calorimetry (TG-DSC, STA-449) was used to investigate the thermal behaviors of the as-synthesized NiMo-$Al_2O_3$ precursors (without calcination). The TG-DSC experiments were carried out under an air atmosphere (20 vol.% $O_2/N_2$) at a heating rate of 20 °C $min^{-1}$.

Scanning electron microscope (SEM) characterizations were carried out on a Hitachi S-4800 instrument, and the accelerating voltage was 15.0 kV.

X-ray fluorescence (XRF) experiments were taken on a PANalytical Axios equipment under a vacuum atmosphere.

### 2.3. Catalytic evaluation

Catalytic reactions of the ordered mesoporous NiMo-$Al_2O_3$ catalysts and reference catalysts towards DBT were carried out in a fixed-bed down-flow stainless-steel reactor (10 mm i.d. and 400 mm long), which is the same to Refs. [4,8]. In short a 0.10 g portion of the catalyst (20–40 mesh) was first diluted with quartz sand (20–40 mesh) to a total volume of 2.5 mL, and then placed in the middle of the reactor. Both ends of the catalyst bed were also packed with quartz sands with the same mesh. The catalyst was in situ pre-sulfided by a liquid stream containing 3.0 wt.% $CS_2$ dissolved in petroleum ether (boiling range from 90 to 120 °C) and $H_2$ at 330 °C and 3.0 MPa for 12 h. Then the reactant, 1.0 wt.% DBT in petroleum ether, was pumped into the reactor. The HDS reactions were carried out in moderate conditions, at a total pressure of 3.0 MPa, a weight hourly space velocity (WHSV) of 96.0 $h^{-1}$, a $H_2$/feed volume ratio of 500, and temperatures of 220 and 240 °C. The liquid HDS product was analyzed by a Agilent 7820 gas chromatograph (flame ionization detector and a 50 m OV101 capillary column) coupled with a quadrupole mass spectrometer (GS–MS).

The specific HDS rate of the catalyst was calculated using the following equation [4,24]:

$$r_{DBT} = \frac{F}{w} \times conv_{DBT} \quad (1)$$

where $r_{DBT}$ is the specific reaction rate of DBT (mol $g^{-1}\,s^{-1}$), $F$ is the molar flow rate of the reactant (mol $s^{-1}$), $w$ is the weight of the catalyst (g), and $Conv_{DBT}$ is the conversion of DBT.

Several products were detected and confirmed by GC–MS in HDS of DBT on the catalysts. The HDS mechanism of DBT

**Table 1**
Abbreviations and pore properties of the ordered mesoporous NiMo-$Al_2O_3$ catalysts.

| Sample | *Abbr.* | $S_{BET}$ ($m^2\ g^{-1}$) | Pore volume ($cm^3\ g^{-1}$) | APD (nm) |
|---|---|---|---|---|
| $Al_2O_3$ | $Al_2O_3$ | 307 | 0.52 | 5.1 |
| 20.0 wt.% $MoO_3/Al_2O_3$ | MoAl | 297 | 0.45 | 4.6 |
| 2.5 wt.% NiO + 20.0 wt.% $MoO_3$ | 2.5NiMoAl | 308 | 0.44 | 4.8 |
| 5.0 wt.% NiO + 20.0 wt.% $MoO_3$ | 5.0NiMoAl | 292 | 0.43 | 4.8 |
| 7.5 wt.% NiO + 20.0 wt.% $MoO_3$ | 7.5NiMoAl | 273 | 0.35 | 4.4 |
| 10.0 wt.% NiO + 20.0 wt.% $MoO_3$ | 10.0NiMoAl | 227 | 0.34 | 4.9 |
| 12.5 wt.% NiO + 20.0 wt.% $MoO_3$ | 12.5NiMoAl | 244 | 0.31 | 4.1 |
| 15.0 wt.% NiO + 20 wt.% $MoO_3$ | 15.0NiMoAl | 239 | 0.33 | 4.2 |

has been fully reported [4,25,26]. In short hydrogenation (HYD) route leads to the formation of a hydrogenated intermediate called tetrahydro-dibenzothiophene (THDBT), and this intermediate further undergoes desulfurization reaction to produce cyclohexylbenzene (CHB). Biphenyl (BP) was produced in direct desulfurization (DDS) route. Compared with our previous results, hexahydro-dibenzothiophene (HHDBT) and bicyclohexane (BCH) were not detected on the ordered mesoporous NiMo-$Al_2O_3$ catalysts [4,26]. To estimate selectivities of the two routes, the following equations were employed [4,24]:

$$\mathrm{DDS} = \frac{BP \times 100\%}{THDBT + BP + CHB} \quad (2)$$

$$\mathrm{HYD} = \frac{(THDBT + CHB) \times 100\%}{THDBT + BP + CHB} \quad (3)$$

## 3.2. Results and discussion

### 3.3. $N_2$ sorption analysis

The $N_2$ adsorption-desorption isotherms and pore size distributions of the ordered mesoporous NiMo-$Al_2O_3$ catalysts are present in Fig. 1. Fig. 1(A) clearly shows that the NiMo-$Al_2O_3$ catalysts have very similar $N_2$ adsorption-desorption isotherms, which are attributed to Type IV [18,19,27]. According to IUPAC classification, the isotherm is ascribed to H1 hysteresis loop [3,19,27]. This is the typical character of the mesoporous materials [19]. The hysteresis loops of the NiMo-$Al_2O_3$ catalysts are very steep at a relative pressure ($P/P_0$) from 0.4 to 0.6, which is caused by the capillary condensation of nitrogen in the mesopores [16,19,28]. At a high relative pressure ($P/P_0 > 0.8$), the nitrogen isotherms of the NiMo-$Al_2O_3$ catalysts end up with nearly horizontal plateaus, indicating the absence of larger pores [16,28]. Compared with the $Al_2O_3$ catalyst, incorporation of 20.0 wt.% $MoO_3$ to the $Al_2O_3$ catalyst (the MoAl catalyst) does not change its original uniform cylindrical pores [18]. Incorporations of various contents of NiO to the MoAl catalyst lead to a trend of diminishing the capillary condensation of nitrogen [3], which is mainly attributed to the high contents of nickel and molybdenum oxides anchored in the mesoporous channels of the alumina. Wang et al. synthesized a series of Ni-Ce-Al catalysts by a similar EISA method, and found that cerium modifications of Ni-Al catalyst led to steeper isotherms and higher condensation [17]. This might be due to the low adding contents of Ni (7 wt.%) and Ce (maximum molar ratio of Ce/(Ce + Al) = 4%) [17]. The $N_2$ adsorption-desorption isotherms of the sulfided ordered mesoporous NiMo-$Al_2O_3$ catalysts are presented in Fig. S1(A). The typical Type IV isotherms with H1 hysteresis loops are confirmed on the sulfided catalysts, indicating that the mesoporous structures are maintained after reactions.

Fig. 1(b) exhibits the pore size distributions of the ordered mesoporous NiMo-$Al_2O_3$ catalysts. Narrow pore size distributions (4–8 nm) are confirmed on the NiMo-$Al_2O_3$ catalysts. A centered peak at 5.0 nm is detected on the $Al_2O_3$ catalyst. The MoAl catalyst shows a similar centered peak as the $Al_2O_3$ catalyst, also at 5.0 nm. After adding various contents of NiO in the synthesis procedure, remarkable changes are detected. As for the 2.5NiMoAl and 5.0NiMoAl the pore size distribution curves become broader than those of the $Al_2O_3$ and MoAl catalysts, and the centered peaks shift to about 5.6 nm. This is similar to the work reported by Wang et al. [17]. Further increasing the contents of NiO to 7.5, 10.0, and 12.5 wt.% lead to splitting of the pore size distribution. The 7.5NiMoAl and 10.0NiMoAl catalysts have two centered peaks at 4.0 and 5.6 nm, while the 12.5NiMoAl catalyst exhibit two centered peaks at 3.8 and 5.0 nm. There is one broad pore size distribution peak (5.0 nm) on the 15.0NiMoAl catalyst. Considering the pore structures of the NiMo-$Al_2O_3$ catalysts and their corresponding compositions, the centered peaks of pore size distribution curves around 5 nm are mainly provided by the ordered mesoporous alumina, while the centered peaks around 4.0 nm might be formed by the pore blockage of the ordered alumina by the active components [12], thus leading the diminishment of the pore sizes. As for the 15.0NiMoAl catalyst splitting disappearance of pore size distribution might be attributed to remarkable pore blockings caused by higher contents of active components. The sulfided ordered mesoporous NiMo-$Al_2O_3$ catalysts have one centered peak around 5.6 nm as revealed in Fig. S1(B).

The pore properties of the ordered mesoporous NiMo-$Al_2O_3$ catalysts, including BET surface area ($S_{BET}$), pore volume, and average pore diameter (APD), are reported in Table 1. High BET surface area, pore volume and APD are detected on the $Al_2O_3$ catalyst, which is 307 $m^2\ g^{-1}$, 0.52 $cm^3\ g^{-1}$, and 5.1 nm, respectively. Adding 20.0 wt.% $MoO_3$ to the $Al_2O_3$ catalyst leads to a small decrease of the BET surface area (from 307 to 297 $m^2\ g^{-1}$, about 3.3%) and obvious decreases of the pore volume (from 0.52 to 0.45 $cm^3\ g^{-1}$, about 13%) and APD (from 5.1 to 4.6 nm, about 9.8%). Further incorporations of various contents of NiO to the MoAl catalyst further decease the BET surface areas and pore volumes, while the average pore distributions of the 2.5NiMoAl, 5.0NiMoAl, and 10NiMoAl catalysts are larger than that of the MoAl catalyst. The pore properties of the sulfided ordered mesoporous NiMo-$Al_2O_3$ catalysts are shown in Table S1. Decreases in BET surface areas and increases in average pore diameters are detected on the sulfided NiMo-$Al_2O_3$ catalysts.

### 3.4. XRD analysis

The ordered mesoporous NiMo-$Al_2O_3$ catalysts were further characterized by XRD (Fig. 2). Fig. 2 (A) shows the small-angle XRD (SXRD) patterns of the NiMo-$Al_2O_3$ catalysts. A visible (100) peak at $2\theta = 1.16^\circ$ is detected on the $Al_2O_3$ catalyst (more evidence is provided by TEM analysis in Section 3.4), and another small (110) peak at $2\theta = 2.12^\circ$ is also confirmed, implying the successful synthesis of hexagonally ordered mesoporous alumina with a space group of *p6 mm* symmetry [16,18,19,29]. According to Bragg equation the distances of $d_{100}$ and $d_{110}$ are 7.6 and 4.2 nm, respectively. Adding 20.0 wt.% of $MoO_3$ in the synthesis procedure maintains the (100) peak, while the small (110) peak cannot be detected by SXRD, indicating that the incorporation of $MoO_3$ affected the long-range order of the mesoporous structures [16]. Further incorporations of

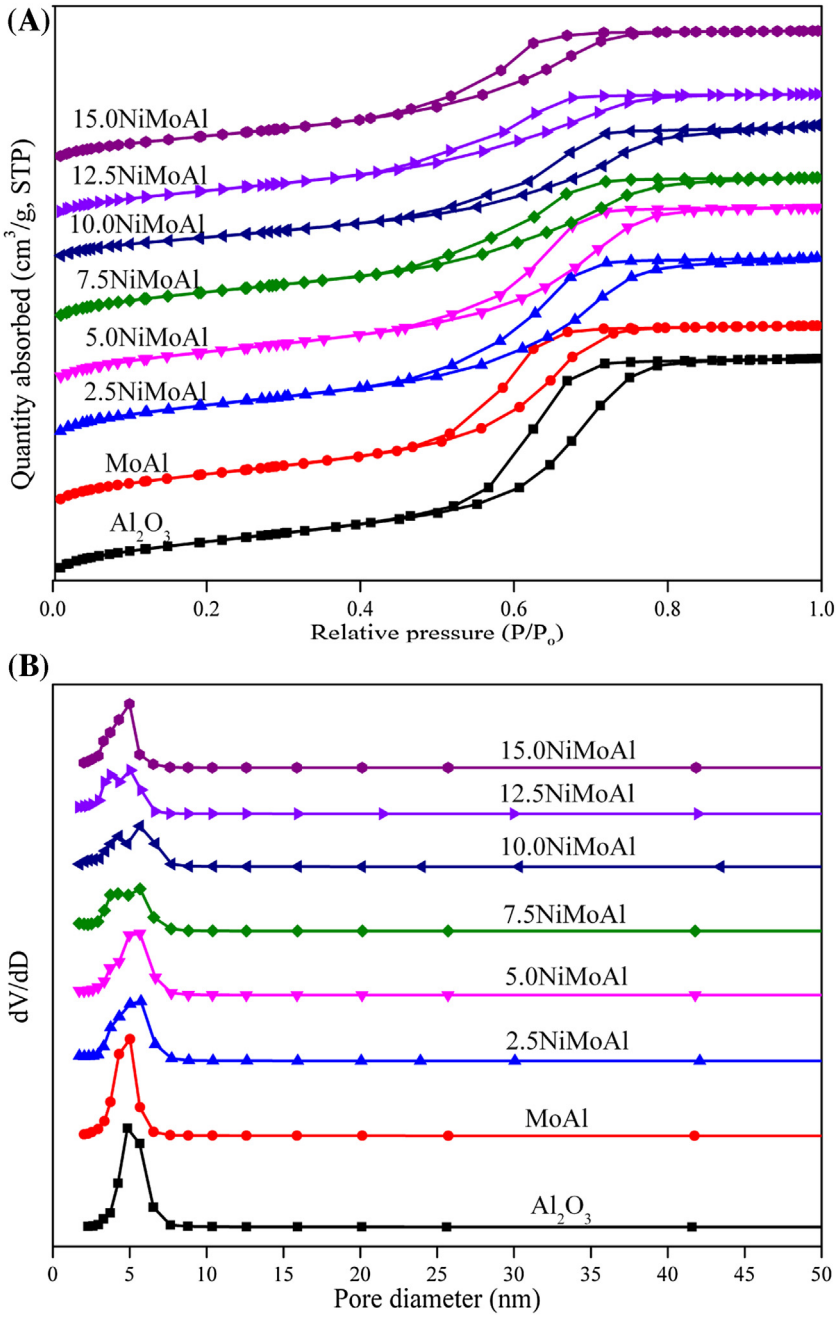


**Fig. 1.** $N_2$ adsorption-desorption isotherms (A) and pore size distributions (B) of the ordered mesoporous NiMo-$Al_2O_3$ catalysts.

various contents of NiO lead to remarkable changes on the SXRD patterns. The characteristic (100) peak of the 2.5NiMoAl catalyst shifts to lower angle value ($2\theta = 1.05$), and no other peaks in the small-angle ranges are detected. The shifts to smaller angle values of the NiMo-$Al_2O_3$ catalysts become more apparent with the increasing contents of NiO, and the 10.0NiMoAl and 12.5NiMoAl catalysts exhibit the (100) peak at $2\theta$ of 0.91°. Besides, the intensities of the (100) peaks tend to be weaker. As for the 15.0NiMoAl catalyst, a very broad (100) peak is detected by SXRD characterization, indicating that the long-range ordered mesoporous structures might partially collapse [3,17]. The SXRD results of the NiMo-$Al_2O_3$ catalysts are in good agreement with the aforementioned $N_2$ adsorption-desorption results, demonstrating the successful synthesis of the ordered mesoporous NiMo-$Al_2O_3$ catalysts by the facile one-pot EISA method.

The phase changes of the NiMo-$Al_2O_3$ catalysts induced by the incorporation of 20.0 wt.% $MoO_3$ and various contents of NiO were investigated by wide-angle XRD (WXRD), and the results are exhibited in Fig. 2(B). The WXRD patterns of the NiMo-$Al_2O_3$ catalysts exhibit no typical XRD peaks attributed to crystalline alumina, which are similar to the results reported by other authors [18,19]. This implies that the amorphous walls are formed on the NiMo-$Al_2O_3$ catalysts [18]. Besides, no XRD peaks due to phases of NiO, $MoO_3$, or other species formed by NiO (or $MoO_3$) with alumina are detected [19]. Soni et at. attributed the absence of XRD signals to the small particle size, which was below the coherence length of X-ray scattering (less than 3–4 nm) [12]. In our present research, even the metal loadings of NiO and $MoO_3$ reach 15.0 and 20.0 wt.%, respectively, no typical XRD peaks are detected (as for the 15.0NiMoAl catalyst), indicating that there are not appar-

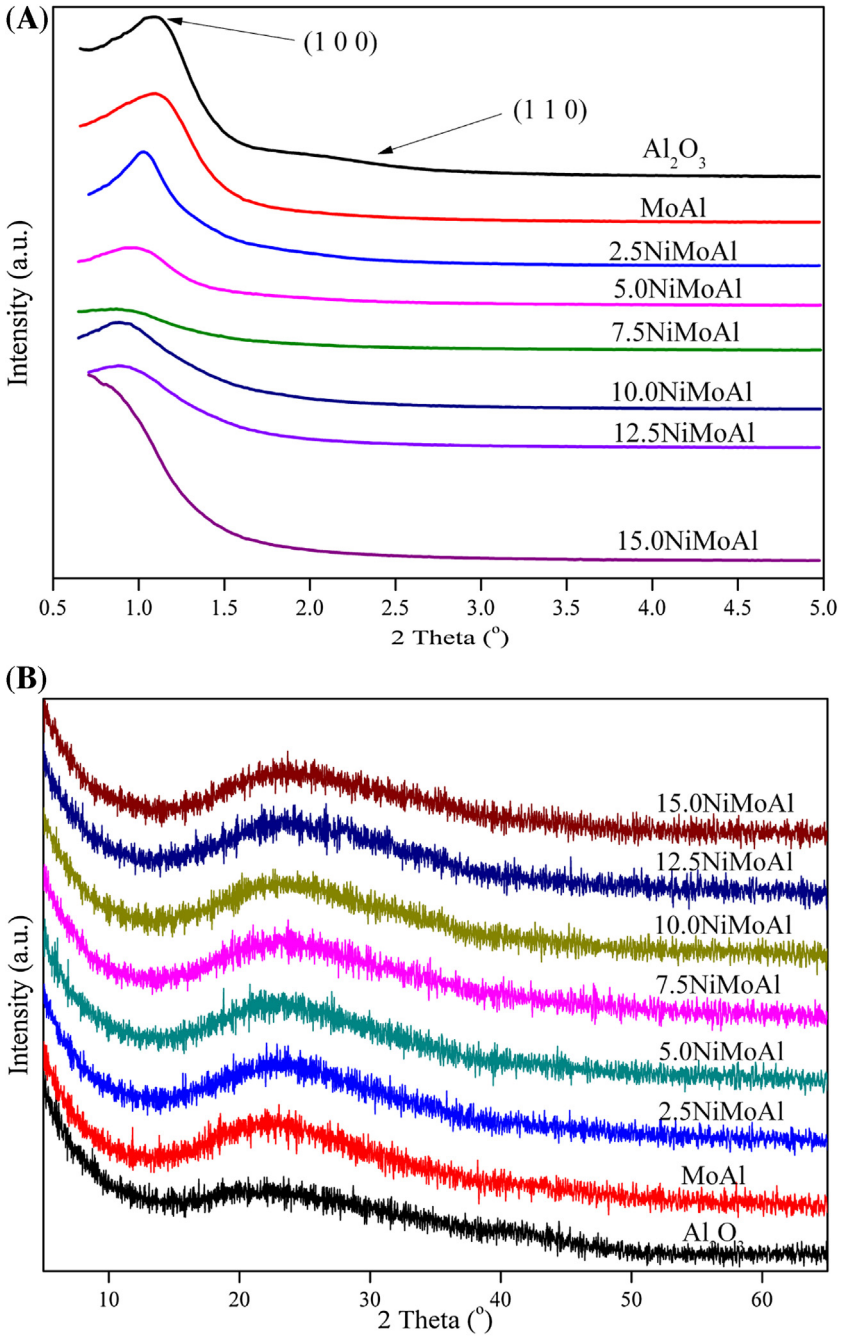


**Fig. 2.** Small-angle XRD (A) and wide-angle XRD (B) patterns of the ordered mesoporous NiMo-$Al_2O_3$ catalysts.

ent agglomerations of these active components in the NiMo-$Al_2O_3$ catalysts. The wide-angle XRD patterns of the sulfided ordered mesoporous NiMo-$Al_2O_3$ catalysts are presented in Fig. S2. No typical XRD peaks attributed to crystalline alumina, molybdenum sulfides, or nickel sulfides are detected on the sulfided catalysts [7,9,18,19].

As aforementioned in Section 2.1 the ordered mesoporous NiMo-$Al_2O_3$ precursors were calcined at 500 °C for 4 h in a static air atmosphere with a ramping temperature of 1 °C $min^{-1}$. The under-mentioned TG-DSC (Section 3.8) and FT-IR (Section 3.9) and FT-IR (Section 3.7) results reveal that the P123 SDA and anhydrous ethanol solvent can be fully removed when the as-synthesized NiMo-$Al_2O_3$ precursors were calcined at 500 °C, and that no phase transformations to crystalline alumina were observed until a temperature as high as 650 °C (TG-DSC analysis). Based on variations in synthesis procedure, sources of aluminum and surfactants, and other important factors (e.g., water content), thermal stabilities of the mesoporous alumina varied distinguishingly [16,18,19,23]. Yuan et al. reported that a phase of γ-$Al_2O_3$ can be obtained at a calcination temperature higher than 800 °C [18], and that increasing calcination temperature led to decreases of BET surface areas and pore volumes of alumina together with broader pore size distributions. This is in agreement with the results reported by Wu et al. [23]. They found that mesoporous alumina calcined at 400 and 500 °C exhibited amorphous frameworks, and that increasing the calcination temperature to 800 °C led to the formation of γ-$Al_2O_3$ [23]. Besides, remarkable losses of BET surface areas and pore volumes were confirmed when calcined at 800 °C [23]. In order to obtain ordered mesoporous NiMo-$Al_2O_3$ catalysts with high surface areas together with a narrow pore size distribution for

homogeneous dispersion of active components, we chose a moderate calcination temperature. Besides, our further research interests are focusing on the effects of ordered mesoporous NiMo-$Al_2O_3$ catalysts with crystalline walls for dispersions of active components and their catalytic performances.

### 3.5. XRF analysis

The chemical compositions of the 10.0NiMoAl and 15.0NiMoAl catalysts were obtained by XRF analysis, and the results are presented in Table S2. The ordered mesoporous NiMo-$Al_2O_3$ catalysts are endowed with desired amounts of components by this modified one-pot EISA method [17,19]. As for the 10.0NiMoAl catalyst the weight percentages of NiO, $MoO_3$, and $Al_2O_3$ are 10.0, 21.0, and 69.0 wt.%, respectively, which is in accordance with the theoretical calculations. The theoretical calculations and chemical compositions of the15.0NiMoAl catalyst are also in good agreement with each other.

### 3.6. TEM analysis

The detailed structures of the ordered mesoporous NiMo-$Al_2O_3$ catalysts after calcination at 500 °C were investigated by TEM, and the results are provided in Fig. 3 and Figs. S3–5. The corresponding fast Fourier transform (FFT) patterns are also exhibited in corresponding figures. Fig. 3 reveals that the ordered mesoporous structures with a regular alignment of cylindrical pores along the (100) direction are apparently confirmed [18,19], which are in good agreement with the results provided by SXRD and $N_2$ adsorption-desorption characterizations. The uniform mesoporous channels around 8.0 nm are observed on the $Al_2O_3$ catalyst, and the diameter of the pore is 5.1 nm, which is in line with the results provided by the $N_2$ sorption (Table 1). Therefore, the thickness of the amorphous alumina wall is about 2.9 nm. As for the MoAl, 5.0NiMoAl, 10.0NiMoAl, and 15.0NiMoAl catalysts, the pore diameters calculated from FFT patterns are 7.4, 9.5, 10.4, and 10.4 nm, respectively. These results are also in accordance with the SXRD results and $N_2$ physisorption. SXRD results reveal that with the increasing contents of NiO in the synthesis procedure, the (100) peaks of the NiMo-$Al_2O_3$ catalysts shift to lower angle sides, indicating that the distances of $d_{100}$ become wider. Table 1 shows that the average pore diameters of the MoAl, 5.0NiMoAl, 10.0NiMoAl, and 15.0NiMoAl catalysts are 4.6, 4.8, 4.9, and 4.2 nm, respectively. Therefore, the thicknesses of the MoAl, 5.0NiMoAl, 10.0NiMoAl, and 15.0NiMoAl catalysts are 2.8, 4.7, 5.5, and 6.2 nm, implying that increasing the contents of NiO in the synthesis form thicker walls of the NiMo-$Al_2O_3$ catalysts. Besides, compared with the $Al_2O_3$ catalyst the mesoporous structure of the 10.0NiMoAl catalyst tends to be partially disorder (Fig. S5). The lengths of the mesoporous channels of the 10.0NiMoAl catalysts are in the range from 40 to 100 nm, which are shorter than those of the $Al_2O_3$ catalyst (200–600 nm as revealed by Fig. S3). This might be due to the incorporations of nickel- and molybdenum-containing compounds, which affect the formation of long-range ordered mesoporous materials, thus leading to short-range ordered mesoporous Ni-Mo-Al nanoparticles. Soni et al. deemed that due to the lack of inter-connected pores, one or two-dimensional mesoporous channels were not so efficient for dispersions of active components, and for diffusions of reactants and products in catalytic reactions [12]. Fig. 4 presents another TEM micrograph of the 10.0NiMoAl catalyst together with the elemental mapping of O, Al, Ni, and Mo. The elemental mappings clearly demonstrate that in the ordered mesoporous 10.0NiMoAl catalyst, the active components NiO and $MoO_3$ are homogeneously dispersed across the whole catalyst.

The HRTEM micrographs of the sulfided 10.0NiMoAl and 15.0NiMoAl catalysts are presented in Figs. 5 and 6, respectively.

**Table 2**
Average length and stacking layers of the $MoS_2$ crystallites.

| Catalyst | Average length (nm) | Average stacking number | $f_{Mo}$ |
|---|---|---|---|
| 10.0NiMoAl | 2.7 | 1.5 | 0.44 |
| 15.0NiMoAl | 4.1 | 2.1 | 0.29 |

After catalytic reactions, the ordered mesoporous structures are maintained. According to the results calculated from FFT results, the pore diameters of the 10.0NiMoAl and 15.0NiMoAl catalysts are 8.5 and 9.4 nm. Compared to the calcined ordered mesoporous NiMo-$Al_2O_3$ catalysts, the decreases of pore diameters might be the agglomerations of metal sulfides. Besides, the typical stacked $MoS_2$ nanoparticles are detected, whose characteristic (002) basal plane has an inter-planar distance about 0.62 nm [3,4,7]. The slab lengths and stacking numbers of the $MoS_2$ nanoparticles on the 10.0NiMoAl and 15.0NiMoAl catalysts are presented in Fig. 7. The slab lengths of the $MoS_2$ nanoparticles on the 10.0NiMoAl catalyst (Fig. 7(A)) are mainly in the range of 2–4 nm, occupying more than 70%, while 50 and 30% of those on the 15.0NiMoAl catalyst are 2–4 and 4–6 nm, respectively. Fig. 7(B) shows that more than 60% of the $MoS_2$ nanoparticles on the 10.0NiMoAl catalyst are monolayer, and more than 50% of the $MoS_2$ nanoparticles are two layers on the 15.0NiMoAl catalyst.

The average slab lengths and stacking layers of the $MoS_2$ nanoparticles on the 10.0NiMoAl and 15.0NiMoAl catalysts were obtained by statistical analysis based on more than 20 micrographs and at least 300 slabs. The average length ($L_{aver.}$) and average stacking layers ($S_{aver.}$) of the $MoS_2$ nanoparticles were calculated according to the equations [13].

$$L_{aver.} = \frac{\sum_{i=1}^{n} x_i L_i}{\sum_{i=1}^{n} x_i} \quad (4)$$

$$S_{aver.} = \frac{\sum_{i=1}^{n} y_i S_i}{\sum_{i=1}^{n} y_i} \quad (5)$$

where $L_i$ is the length of slab i, $S_i$ is the number of layers in slab i, $x_i$ is the number of slabs within length $L_i$, and $y_i$ is the number of slabs with $S_i$ layers.

In order to estimate the dispersion of the $MoS_2$ nanoparticles, the average fraction of molybdenum atoms on the edge surface of the $MoS_2$ crystallines ($f_{Mo}$) were calculated according to the following equation, assuming that the $MoS_2$ crystallines are perfect hexagons [13,30]:

$$f_{Mo} = \frac{\sum_{i=1}^{m} (6n_i - 6)}{\sum_{i=1}^{m} (3n_i{}^2 - 3n_i + 1)} \quad (6)$$

where $n_i$ is the number of Mo atoms along one edge of a $MoS_2$ slab calculated from its length ($L_i = 3.2(2n_i - 1)$Å), and $m$ is the total number of slabs in HRTEM micrographs. The calculated average length ($L_{aver.}$), average stacking ($S_{aver.}$) crystalline, and dispersion ($f_{Mo}$) of $MoS_2$ crystalline are reported in Table 2.

The average lengths ($L_{aver.}$) of the 10.0NiMoAl and 15.0NiMoAl catalysts are 2.7 and 4.1 nm, respectively, and the average stacking numbers ($S_{aver.}$) of the 10.0NiMoAl catalyst is 1.5, which is a little shorter than that on the 15.0NiMoAl catalyst (2.1). Besides, the $MoS_2$ dispersion on the 10.0NiMoAl catalyst is higher than that on the 15.0NiMoAl catalyst, which are 0.44 and 0.29, respectively.

### 3.7. SEM analysis

The morphology changes induced by incorporations of various contents of NiO to the MoAl catalyst were studied by SEM, and the results are exhibited in Fig. S6. The MoAl nanoparticles (Fig. S6(A)) are stacked in parallel, and the length of the nanoparticles is about

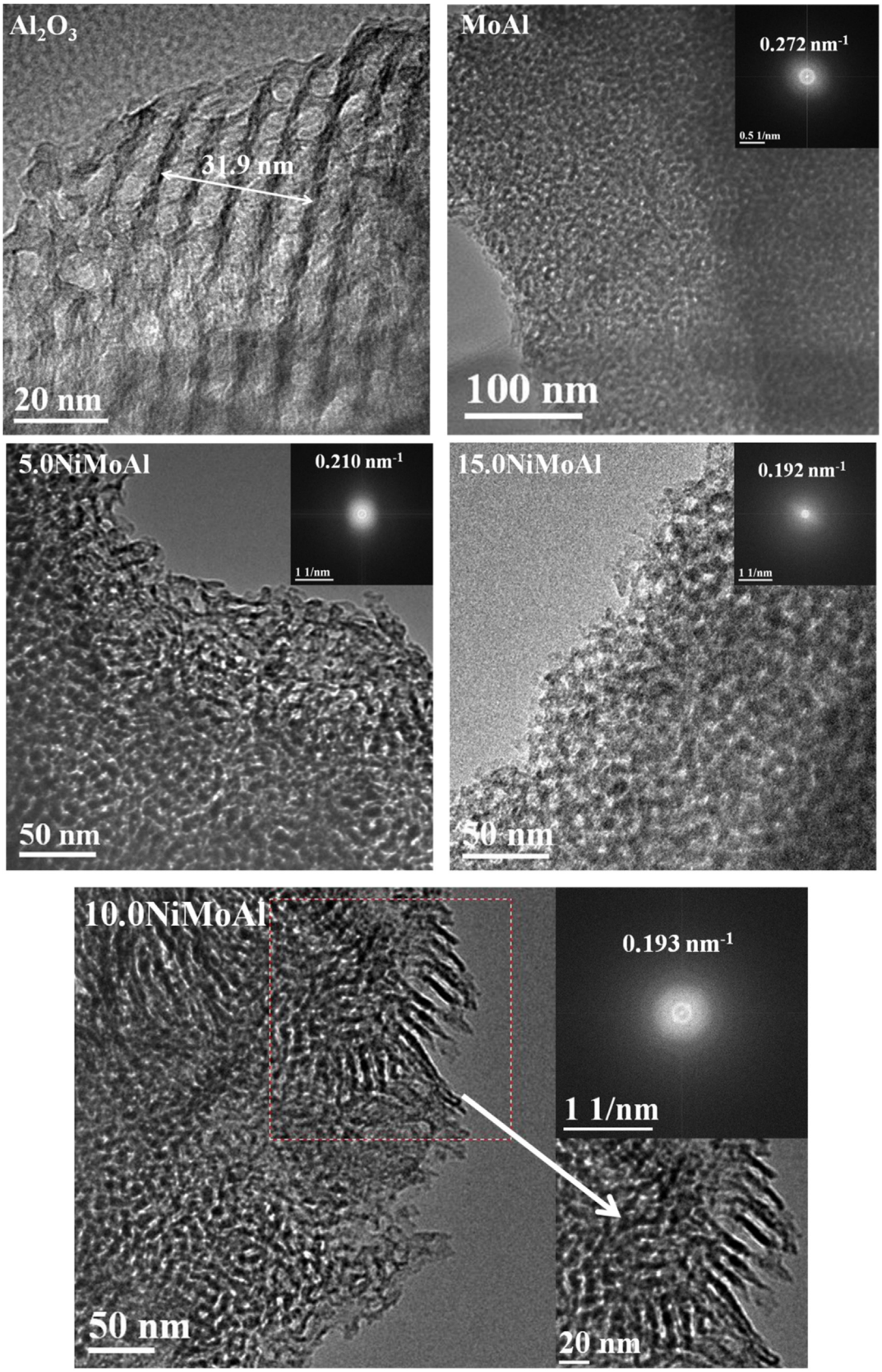


**Fig. 3.** TEM micrographs of the ordered mesoporous NiMo-$Al_2O_3$ catalysts.

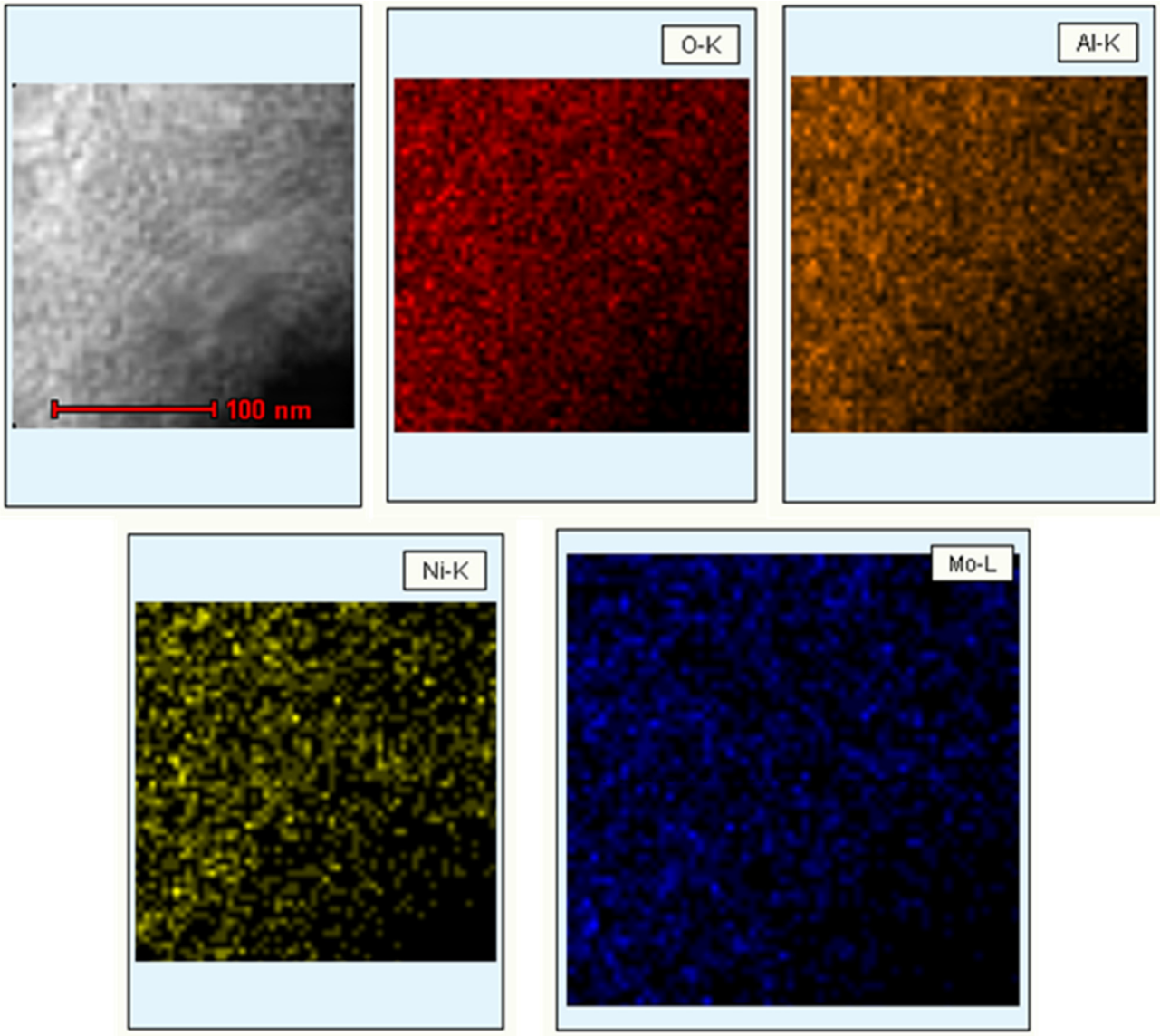


**Fig. 4.** TEM micrograph of the 10.0NiMoAl catalyst and the elemental mapping of O, Al, Ni, and Mo.

150 nm. Incorporation of 5.0 wt.% NiO in the synthesis procedure remarkably affected the morphologies (Fig. S6(B)). Few long-range parallel nanoclusters are detected. Instead, the 5.0NiMoAl catalyst exhibits dis-orderly stacked nanoparticles. As for the 10.0NiMoAl catalyst the nanoparticles tend to agglomerate to form much bigger ones, and some smaller nanoparticles could still be detected. The 15.0NiMoAl catalyst shows irregular crystalline nanoparticles, which are much different to other NiMo-$Al_2O_3$ catalysts.

### 3.8. TG-DSC analysis

Thermal behaviors of the ordered mesoporous NiMo-$Al_2O_3$ precursors (without calcination) in an $O_2/N_2$ (20/80, v/v) atmosphere were investigated by TG-DSC analysis, and the results are presented in Fig. 8. The $Al_2O_3$, MoAl, and 10.0NiMoAl precursors show similar TG-DSC curves, which are composed of one endothermic and three main exothermic peaks together with corresponding weight losses. Take the analysis of the $Al_2O_3$ precursor as sample. The endothermic peak around 115 °C comes first, and the weight loss is around 2.0 wt.%. This peak is mainly ascribed to the desorptions of physically adsorbed water [3,31,32]. The first exothermic peak is around 150 °C and the weight loss is around 20.0 wt.%, which is attributed to the fragmentation of the anhydrous ethanol solvent and the triblock copolymer P123 [33]. Then follows another exothermic peak centered at 280 °C. This peak is associated with the oxidation of the carbonaceous species produced at lower temperatures [31,33,34]. The weight losses of the $Al_2O_3$, MoAl, and 10.0NiMoAl precursors during this step are 42.2, 31.8, and 26.1 wt.%, respectively. Differences in weight losses of these precursors are mainly attributed to the incorporations of 20.0 wt.% $MoO_3$ and 10.0 wt.% NiO in the synthesis procedure. The final exothermic peak ends before 500 °C, which is due to the further oxidation of the remaining organic template in strong interactions with the amorphous walls [33], and the weight loss is around 15 wt.%. The TG-DSC results confirm that the decomposition and complete removal of the SDA P123 and other compounds would end before 500 °C. Besides, the ordered mesoporous NiMo-$Al_2O_3$ catalysts show a high thermal stability, because no endothermic or exothermic peaks together with weigh loss peaks occur, even the temperature reaching as high as 650 °C.

Kleitz et al. synthesized a series of alumina using various surfactants and studied their thermal behaviors [31]. They proposed that endothermic evaporations, thermo-desorption, and oxidative

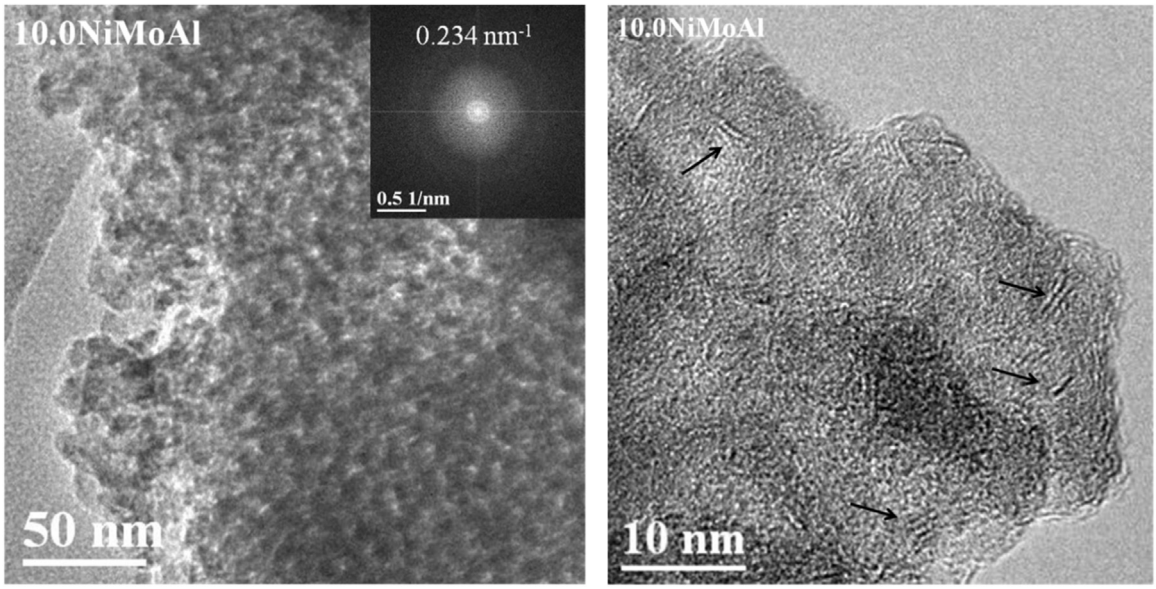


**Fig. 5.** HRTEM micrograph of the sulfided 10.0NiMoAl catalyst.

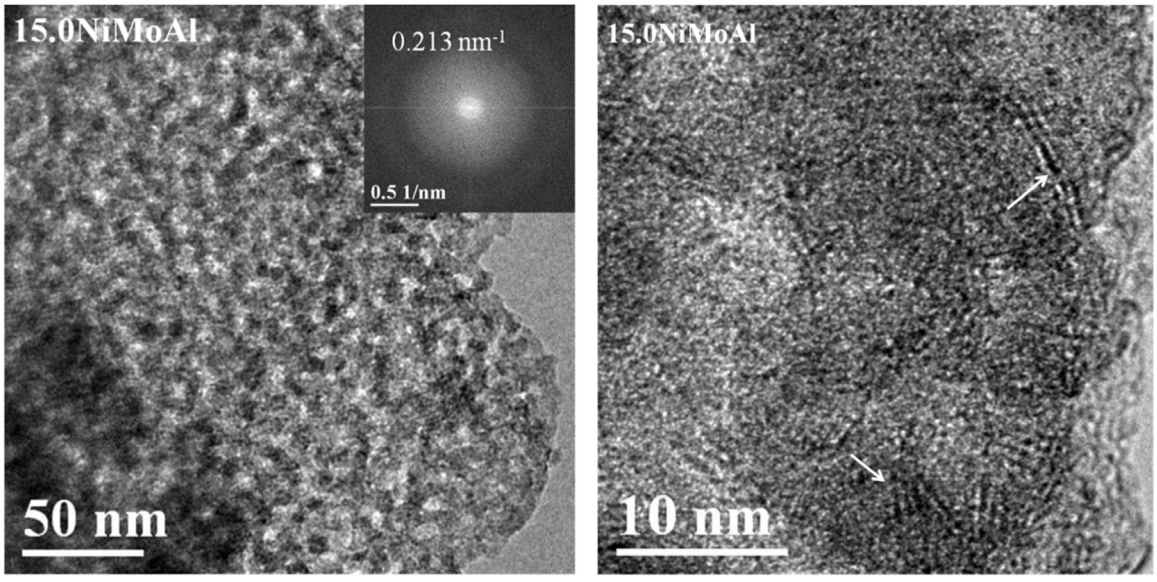


**Fig. 6.** HRTEM micrograph of the sulfided 15.0NiMoAl catalyst.

decomposition could simultaneously occur, thus leading overlapped signals in the DTA curves [31]. Therefore, it seemed very challenging to attribute each endothermic or exothermic peak to a specific thermal behavior. The thermal behaviors of the ordered mesoporous NiMo-$Al_2O_3$ catalysts in our research are, to some extent, even more complicated than those reported by other groups [31–34], because not only the thermal behaviors summarized by Kleita et al., but also the incorporations of various contents of NiO, $MoO_3$, and solvent (anhydrous ethanol) and their interactions, also play important roles in the thermal behaviors of the ordered mesoporous NiMo-$Al_2O_3$ catalysts.

### 3.9. FT-IR analysis

The ordered mesoporous NiMo-$Al_2O_3$ catalysts exhibit similar FT-IR spectra as shown in Fig. S7. A broad FT-IR peak around 3450 $cm^{-1}$ is confirmed, which might be due to the stretching vibrations of adsorbed water [35,36], and this interaction also exhibits another bending mode at 1630 $cm^{-1}$ [35,36]. Another FT-IR peak around 610 $cm^{-1}$ is characteristic of octahedral aluminum [36,37]. The peaks ranging from 500 to 900 $cm^{-1}$ might be attributed to the bonds of Al—O [35–37]. Furthermore, FT-IR results also confirm that the solvent (anhydrous ethanol), SDA (P123), and other compounds ($HNO_3$ and isopropoxide groups) were fully removed after calcination of the ordered mesoporous NiMo-$Al_2O_3$ precursors at 500 °C for 4 h. Compared to our previous reports and other reports [4,8,12,26], no FT-IR peaks due to the bonds of Mo—O (finger-like FT-IR peaks from 1000 to 700 $cm^{-1}$) or Ni—O are detected, implying that nickel- and molybdenum-containing compounds were incorporated into the channels of the ordered mesoporous alumina.

Based on the aforementioned results and relevant researches [17–19], a possible formation mechanism of the ordered mesoporous NiMo-$Al_2O_3$ catalysts by this facile EISA method is proposed in Scheme 1. The structure-directing agent P123 was dissolved in anhydrous ethanol to form a micellar solution. Then the hydrophilic

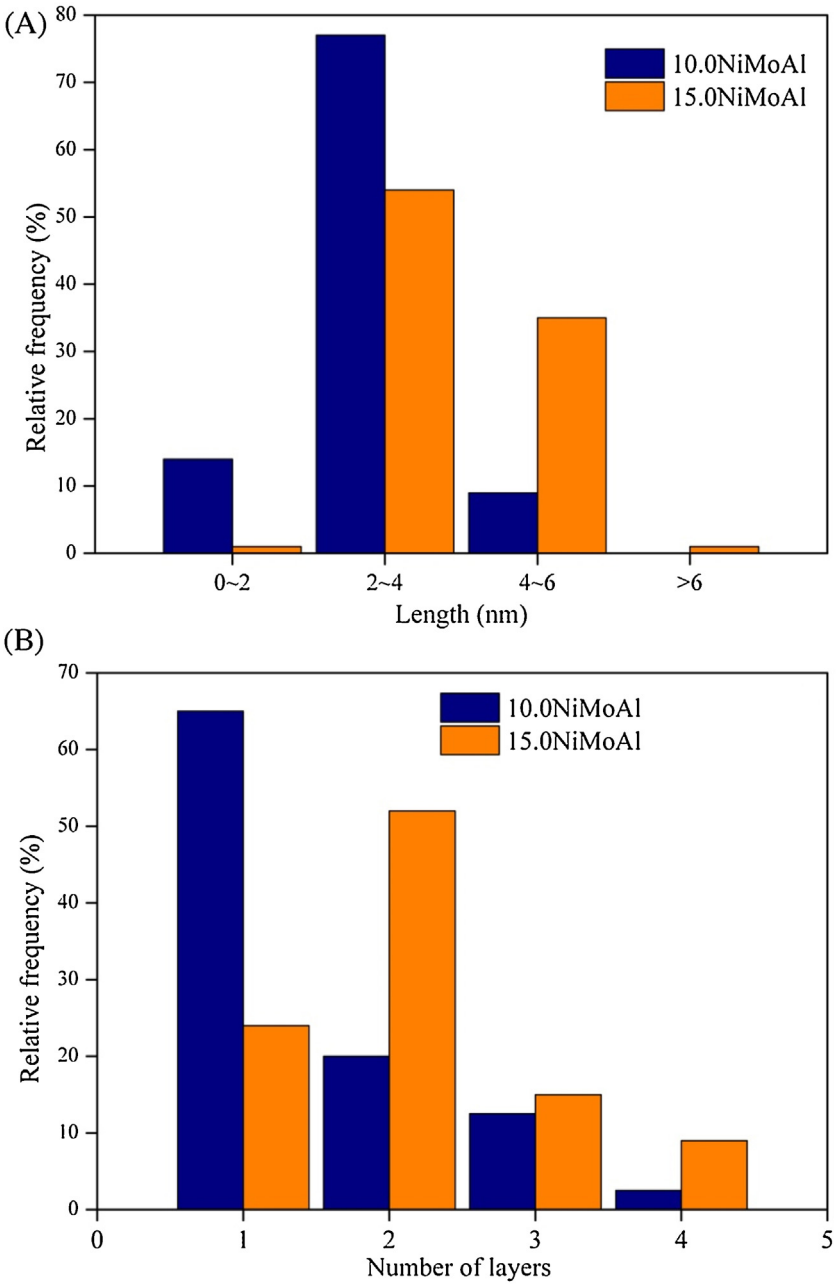


**Fig. 7.** Lengths (A) and stacking numbers (B) distributions of the $MoS_2$ crystallines on the 10.0NiMoAl and 15.0NiMoAl catalysts.

Al-, Ni-, and Mo-containing species can preferentially precipitate around the hydrophilic corona of the P123 micelles. When evaporating the solvent anhydrous ethanol, the condensation of the Al-, Ni-, and Mo- containing species around the surfactant P123 micelle and the self-assembly of these species proceeded simultaneously. This would lead to a hexagonally mesoporous structure (*p6mm* symmetry). After the removal of surfactant and other compounds through calcination in air at 500 °C for 4 h, the corresponding metal oxides were obtained. The alumina served as the stable ordered mesoporous skeleton, while $MoO_3$ and NiO homogeneously anchored into the channels of alumina.

### 3.10. TPR analysis

The ordered mesoporous NiMo-$Al_2O_3$ catalysts were further characterized by $H_2$-TPR to study their reductive abilities, and the $H_2$-TPR patterns are present in Fig. 9. Various reductive abilities are detected after the incorporations of various contents of NiO. The MoAl catalyst has two main hydrogen consumption peaks at 560 and 840 °C. The former TRP peak is attributed to the reduction of Mo-containing species from $Mo^{6+}$ to $Mo^{4+}$ [4,12,38–40], and the latter is assigned to the further reduction from $Mo^{4+}$ to $Mo^0$ [12,41,42]. The relative intensity for $Mo^{4+}$ to $Mo^0$ is more intense than that for $Mo^{6+}$ to $Mo^{4+}$, which is attributed to a strong interaction between the Mo species and the support [14,40]. As for the tri-metal Ni-Mo-Al catalysts, incorporations of various contents of NiO in the synthesis procedure lead to the formation of a new TPR peak. As for the 2.5NiMoAl and 5.0NiMoAl catalysts, the newly formed TPR peak at 470 °C is mainly ascribed to the reduction of NiO particles [43]. Due to the small amounts of NiO additions, these two TPR peaks are relatively weak. The following broad hydrogen consumption peak from 550 to 750 °C can be attributed to the partial

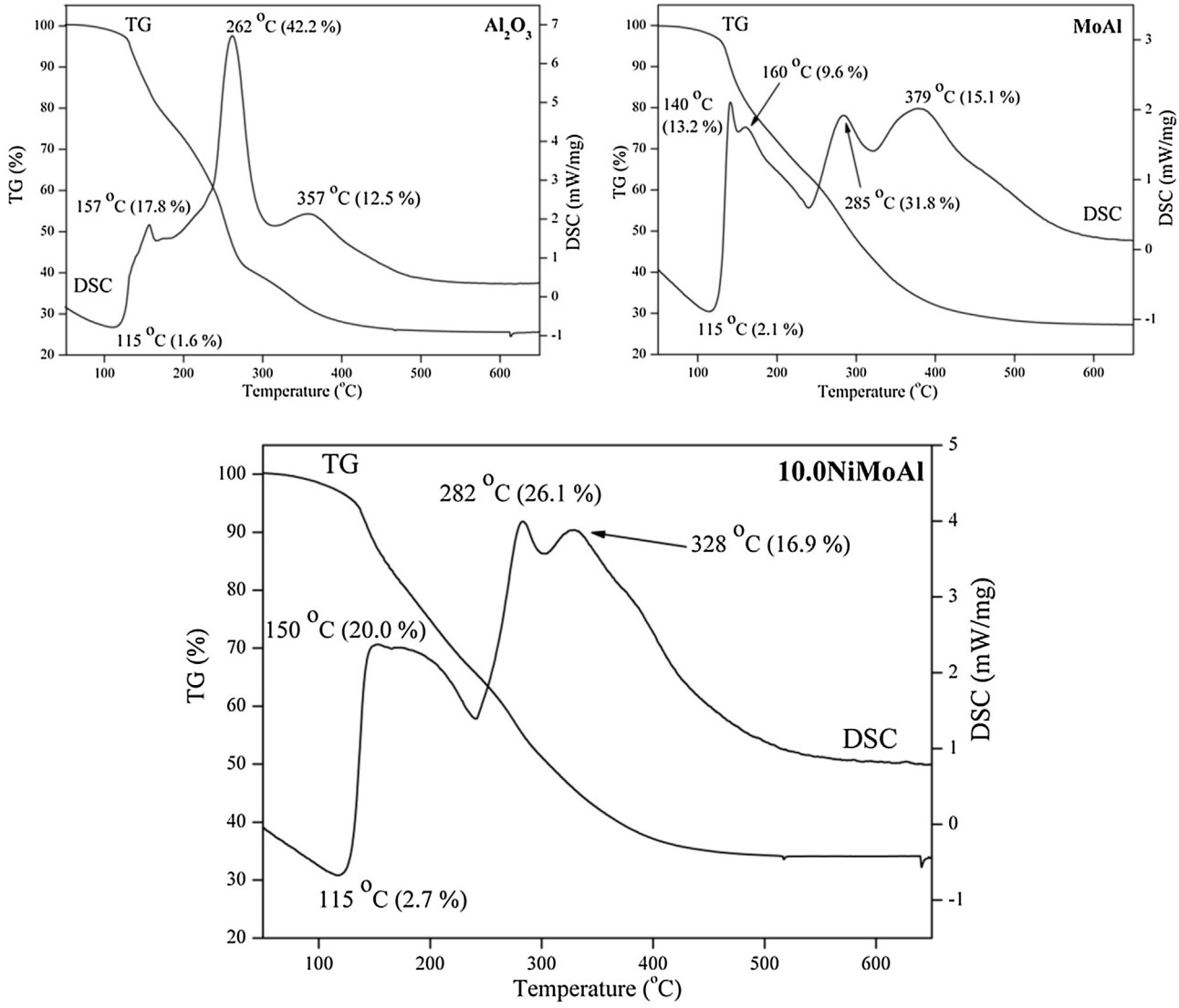


**Fig. 8.** TG-DSC curves of the as-synthesized NiMo-$Al_2O_3$ precursors.

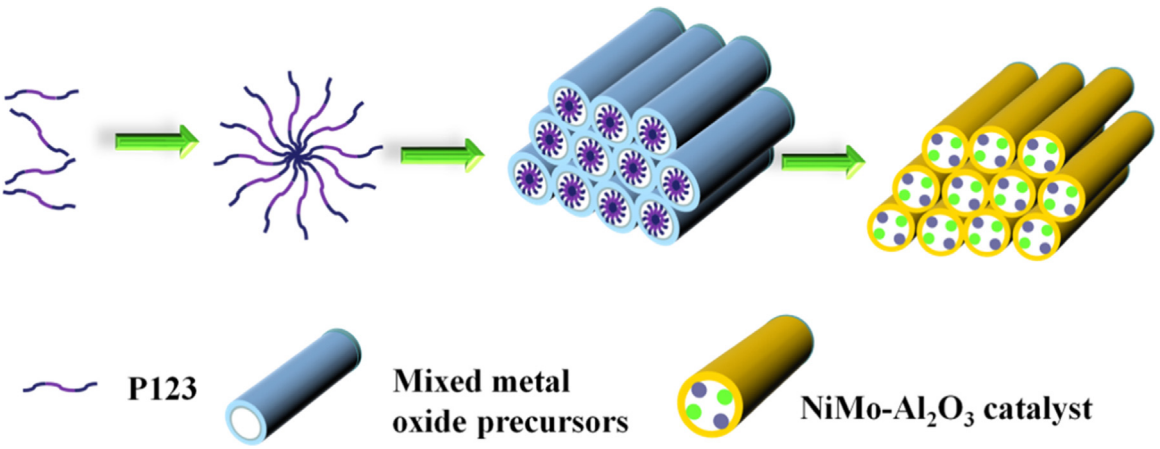


**Scheme 1.** Possible formation mechanism of ordered mesoporous NiMo-$Al_2O_3$ catalysts.

reduction of molybdate (from $Mo^{6+}$ to $Mo^{4+}$) [41,42]. The high-temperature TPR peaks (higher than 750 °C) of the 2.5NiMoAl and 5.0NiMoAl catalysts are also attributed to the reduction of Mo-containing species from $Mo^{4+}$ to $Mo^0$ [41]. Besides, the TPR peaks attributed to molybdate from $Mo^{4+}$ to $Mo^0$ tend to be a little smaller with a comparison to that of the MoAl catalyst, indicating that the incorporations of NiO lead to an easy reduction of the Mo species. As for the 7.5NiMoAl catalyst the TPR profile is very similar to those

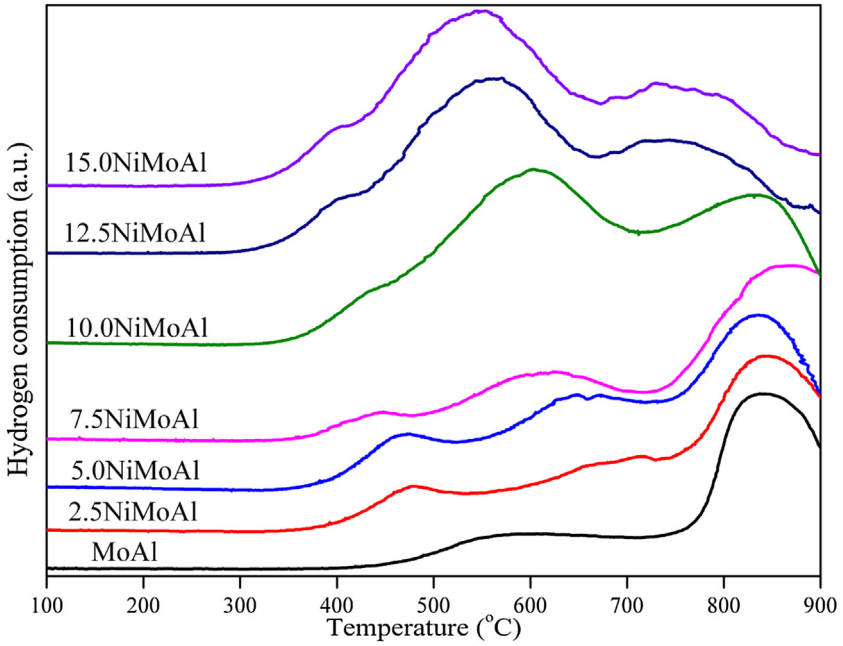


**Fig. 9.** TPR patterns of the ordered mesoporous NiMo-$Al_2O_3$ catalysts.

of the 2.5NiMoAl and 5.0NiMoAl catalysts. However, the centered temperatures of hydrogen consumption peaks shift to the low temperature range, which might be due to the various interactions between the active components and the alumina support [41,43]. Increasing the contents of NiO to 10.0, 12.5, and 15.0 wt.% in the synthesis procedure lead to remarkable changes of the TPR profiles, and these three catalysts exhibit similar patterns. Three main TPR peaks are detected, whose profiles are different to those of the other NiMoAl catalysts. An intense hydrogen consumption peak is detected at 550 °C for the 12.5NiMoAl and 15.0NiMoAl catalysts (600 °C for the 10.0NiMoAl catalyst). Accompanied by the intense TPR peak, a small TPR peak is also detected around 400 °C (420 °C for the 10.0NiMoAl catalyst). Another broad but not intense TPR peak is centered in the temperature range from 700 to 900 °C. The small TPR peak (around 400 °C) is due to the reduction of NiO nanoparticles [19], and this kind of NiO is not strongly bonded to the support [41]. The intense TPR peak (around 550 °C) is mainly attributed to the reduction of Mo-containing species, followed by the broad TPR peak (higher than 700 °C), which is also attributed to consecutive reduction of $Mo^{4+}$ to lower state [13,38].

The TPR results reveal that incorporations of NiO to the MoAl catalyst efficiently affect both the TPR profiles and centered temperatures of the ordered mesoporous NiMo-$Al_2O_3$ catalysts. With the adding amounts of NiO to no more than 7.5 wt.% in our present work (referring to the 2.5NiMoAl, 5.0NiMoAl, and 7.5NiMoAl catalysts), a small TPR peak (around 470 °C) due to the reduction of NiO species is detected, and the high temperature TPR peaks of the Mo species (>750 °C) tend to be smaller. Further increasing the contents of NiO to 10.0, 12.5, and 15.0 wt.% lead to remarkable changes of the reductive abilities of the nickel- and molybdenum-containing species. The main reduction peaks due to molybdenum and nickel oxides shift to lower temperature (550–600 °C) and become more intense, which implies that the incorporated NiO results in a strong interaction between the nickel and molybdenum species [12,40]. This is similar to the results reported by Wang et al. [40]. They found that introductions of Ni species to a Mo/MCM-41 catalyst led to shift, split, and disappearance of the Mo reduction peaks, which were ascribed to the interaction between the metal species, and to the hydrogen spillover from nickel sites to molybdenum sites [40]. Consequently, the high temperature reduction peaks (higher than 750 °C) of the Mo species tend to be much smaller. Previous researches revealed that the reduction of molybdate in an octahedral site was easier than that in a tetrahedral site [4,14,44,45]. Therefore, the main TPR peaks (550–600 °C) of the 10.0NiMoAl, 12.5NiMoAl, and 15.0NiMoAl catalysts might be attributed to reduction of molybdate in octahedral sites.

### 3.11. Catalytic results

The catalytic activity of the ordered mesoporous NiMo-$Al_2O_3$ catalysts and two reference catalysts (NiMo/meso-$Al_2O_3$ and NiMo/γ-$Al_2O_3$) was evaluated in the HDS reaction. DBT, a typical sulfur-containing compound, was chosen as the model compound [46]. It has been widely reported that DBT undergoes two main routes in HDS reactions [4,25,39,40,46,47]. One route is called DDS. In this route the sulfur atom of DBT is eliminated to form BP through a two-step reaction, thus yielding unsaturated hydrocarbons. The other route is called HYD. During this route DBT first reacts with hydrogen to form hydrogenated intermediates TH-DBT and HH-DBT, and then the sulfur is removed to produce CHB. Besides, DBT might also be fully hydrogenated to yield another intermediate called dodecahydro-dibenzothiophene (DH-DBT), and then the sulfur is removed to form BCH [26,47]. The catalytic results of the catalysts at 220 and 240 °C are reported in Tables 3 and 4. The HDS products of DBT on the ordered mesoporous NiMo-$Al_2O_3$ catalysts are TH-DBT, BP, and CHB, while a small amount of HHDBT is detected on the NiMo/γ-$Al_2O_3$ catalyst. The hydrogenated intermediates (HH-DBT, DH-DBT) and the fully hydrogenated product BCH are not detected on the ordered mesoporous NiMo-$Al_2O_3$ catalysts. Previous results reveal that hydrogenation of TH-DBT to HH-DBT (or dehydrogenation of HH-DBT to TH-DBT) on a NiMo/γ-$Al_2O_3$ catalyst was the fastest reaction step in HDS of DBT [25]. Besides, no catalytic cracking products were detected due to the low reaction temperatures and high WHSV. The specific reaction rates, and the ratios of HYD/DDS routes were calculated according to Eqs. (1)–(3), and the results are also reported in Tables 3 and 4.

Tables 3 and 4 reveal that increasing reaction temperatures from 220 to 240 °C play a salutary role in improving the activities

**Table 3**
Catalytic results of the ordered mesoporous NiMo-$Al_2O_3$ catalysts reacted at 220 °C.

| | Conversion (%) | TH-DBT | BP | CHB | *rate* ($10^{-9}$ × mol $g^{-1}$ $s^{-1}$) | HYD/DDS |
|---|---|---|---|---|---|---|
| 2.5NiMoAl | 12.1 | 9.1 | 87.6 | 3.3 | 175 | 0.14 |
| 5.0NiMoAl | 16.9 | 2.4 | 97.0 | 0.1 | 245 | 0.03 |
| 7.5NiMoAl | 21.0 | 2.9 | 95.2 | 1.9 | 305 | 0.05 |
| 10.0NiMoAl | 22.5 | 2.2 | 95.6 | 2.2 | 326 | 0.05 |
| 12.5NiMoAl | 12.1 | 3.3 | 95.0 | 1.7 | 175 | 0.05 |
| 15.0NiMoAl | 10.0 | 5.0 | 95.0 | 0 | 145 | 0.05 |
| NiMo/γ-$Al_2O_3$ | 8.2 | 26.1[a] | 63.8 | 10.1 | 119 | 0.57 |
| NiMo/meso-$Al_2O_3$ | 5.2 | 7.1 | 86.2 | 6.7 | 75 | 0.16 |

[a] 22.0% THDBT + 4.1% HHDBT

**Table 4**
Catalytic results of the ordered mesoporous NiMo-$Al_2O_3$ catalysts reacted at 240 °C.

| | Conversion (%) | TH-DBT | BP | CHB | *rate* ($10^{-9}$ × mol $g^{-1}$ $s^{-1}$) | HYD/DDS |
|---|---|---|---|---|---|---|
| 2.5NiMoAl | 20.9 | 4.9 | 89.5 | 5.6 | 303 | 0.12 |
| 5.0NiMoAl | 26.7 | 2.6 | 94.7 | 2.7 | 387 | 0.06 |
| 7.5NiMoAl | 28.5 | 2.8 | 93.3 | 3.9 | 413 | 0.07 |
| 10.0NiMoAl | 32.5 | 1.8 | 95.4 | 2.8 | 471 | 0.05 |
| 12.5NiMoAl | 21.7 | 1.8 | 92.6 | 5.6 | 315 | 0.08 |
| 15.0NiMoAl | 19.5 | 2.6 | 93.8 | 3.6 | 283 | 0.07 |
| NiMo/γ-$Al_2O_3$ | 14.1 | 8.9[a] | 72.3 | 18.8 | 205 | 0.38 |
| NiMo/meso-$Al_2O_3$ | 9.7 | 3.8 | 81.8 | 14.4 | 141 | 0.22 |

[a] 7.6% THDBT + 1.3% HHDBT

of the ordered mesoporous NiMo-$Al_2O_3$ catalysts and the reference catalysts. The conversions of DBT on the 15.0NiMoAl catalyst reached 10.0 and 19.5% at 220 and 240 °C, respectively, indicating that the activity of the 15.0NiMoAl catalyst was almost doubled by a temperature increase of 20 °C. Among the ordered mesoporous NiMo-$Al_2O_3$ catalysts the 15.0NiMoAl catalyst has a lower activity at evaluated HDS conditions, while the 10.0NiMoAl catalyst shows a higher activity towards DBT than the other NiMo-$Al_2O_3$ catalysts, which can convert 22.5 and 32.5% DBT at 220 and 240 °C, respectively. Tables 3 and 4 also reveal that all the ordered mesoporous NiMo-$Al_2O_3$ catalysts have higher conversions of DBT than the reference NiMo/meso-$Al_2O_3$ and NiMo/γ-$Al_2O_3$ catalysts. Besides, very low conversions were detected on the ordered mesoporous MoAl catalyst as shown in Table S3, which can only convert 0.7 and 2.4% DBT even at higher reaction temperatures of 260 and 280 °C, respectively.

Tables 3 and 4 show that BP is the abundant product in HDS of DBT on the ordered mesoporous NiMo-$Al_2O_3$ catalysts, occupying more than 85% of the HDS products. Therefore, the NiMo-$Al_2O_3$ catalysts show very low ratios of HYD/DDS routes. The ratios of HYD/DDS routes were calculated to compare the product selectivities on the ordered mesoporous NiMo-$Al_2O_3$ catalysts. The 2.5NiMoAl catalyst has a higher HYD/DDS ratio than the other NiMo-$Al_2O_3$ catalysts, both at 220 and 240 °C, which are 0.14 and 0.12, respectively. Increasing reaction temperature from 220 to 240 °C leads to higher HYD/DDS ratios expect the 2.5NiMoAl and 10.0NiMoAl catalysts, which is in accordance with previous results [40]. The ratios of HYD/DDS routes of the other NiMo-$Al_2O_3$ catalysts vary from 0.03 to 0.08. Among all the catalyst the NiMo/γ-$Al_2O_3$ catalyst has higher HYD/DDS ratios, which reaches 0.57 and 0.38 at 220 and 240 °C, respectively. Wang et al. found that the HYD/DDS ratios decreased with increasing reaction temperatures [40]. Prins and coworkers reported that the DDS route was the predominant way in HDS of DBT [25,47,48], and that the rate constant of DDS route was 3.2 times larger than that of the HYD route [25]. The ratios of HYD/DDS routes reaching 0.17 and 0.11 were detected on a NiMo/γ-$Al_2O_3$ catalyst at 300 and 340 °C, respectively [48]. Introduction of Ni promoter to the $MoS_2$ catalyst enhances desulfurization rates, both in the DDS route and in the desulfurization step of the hydrogenated intermediate in the HYD route [25]. According to Density Functional Theory (DFT) calculations and as for the Ni promoted $MoS_2$ catalyst, the nickel atoms are coordinated by four sulfur atoms forming a square-planar morphology at the (10−10) metal edges, and are in a tetrahedral site or in a square-planar sulfur coordination at the (−1010) sulfur edges [25,49]. The square-planar nickel atoms are very accessible to sulfur-containing compounds, thus showing a high desulfurization activity [25]. Tables 3 and 4 also reveal that due to the high desulfurization activity of the ordered mesoporous NiMo-$Al_2O_3$ catalysts no hydrogenated intermediate HH-DBT is detected, and that the ratios of HYD/DDS routes are quite low (0.03–0.14).

Among the ordered mesoporous NiMo-$Al_2O_3$ catalysts, the 10.0NiMoAl catalyst exhibit higher specific reaction rates towards HDS of DBT, reaching 326 and 471 × $10^{-9}$ mol $g^{-1}$ $s^{-1}$ at 220 and 240 °C, respectively. Since the main difference for preparing the ordered mesoporous NiMo-$Al_2O_3$ catalysts is the weight content of NiO, the atomic ratio $R$ ($R$ = Ni/(Ni + Mo)) is employed in order to correlate the contents of NiO with the specific reaction rates [50,51], and the result is depicted in Fig. 10.

Fig. 10 shows that a trend of enhanced HDS activities is observed with the increasing $R$ values up to no more than 0.4 in the ordered mesoporous NiMo-$Al_2O_3$ catalysts (referring to the 2.5NiMoAl, 5.0NiMoAl, and 7.5NiMoAl catalysts). This trend is mainly assigned to the promoting effect of nickel, as revealed by the TPR results. Fig. 9 shows that the 2.5NiMoAl, 5.0NiMoAl, and 7.5NiMoAl catalysts exhibit similar TPR patterns. A very small TPR peak attributed to the reduction of NiO is confirmed around 470 °C, while the main reduction of molybdate at temperature higher than 750 °C changes a little and shifts to low temperature range. This indicates that small amounts of incorporated NiO have some interactions with molybdate [40], thus leading to enhanced catalytic activities in HDS of DBT. As for the 10.0NiMoAl, 12.5NiMoAl, and 15.0NiMoAl catalysts, the TPR peaks attributed to molybdate apparently shift to lower temperatures (550–600 °C) and become very intensely, while the high-temperature reduction peaks (more than 750 °C) assigned to the Mo species tend to be much smaller. The changes in centered temperatures and relative intensities of the 10.0NiMoAl, 12.5NiMoAl, and 15.0NiMoAl catalysts are due to increasing contents of the incorporated NiO in the synthesis procedure, which remarkably lead to an obvious interaction between the nickel and molybdenum species [12,40]. Besides, Wang et al. pointed out that for every series of HDS catalysts, there existed one optimal

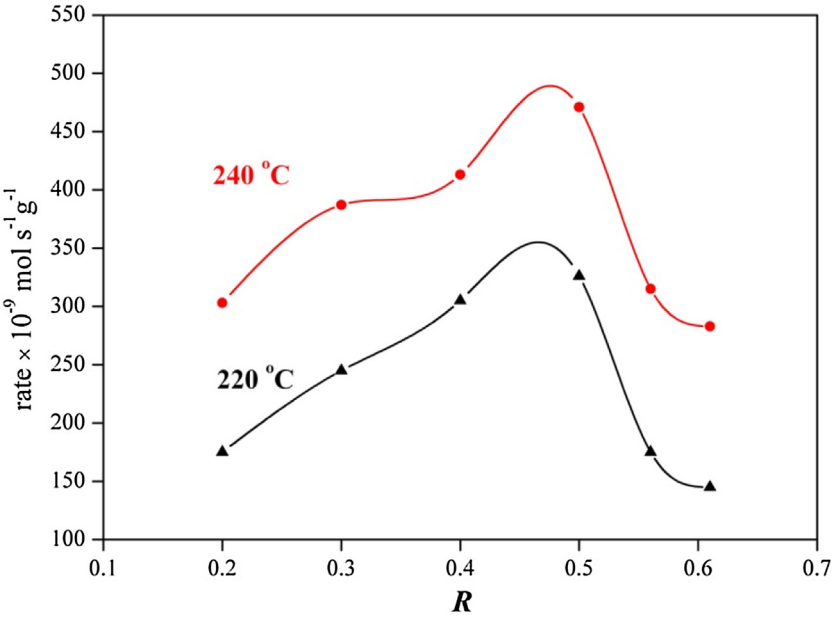


**Fig. 10.** Comparison between the *R* values and the specific reaction rates of the ordered mesoporous NiMo-$Al_2O_3$ catalysts.

Co/Mo molar ratio [39], which were affected by the active components, supports, preparation procedures, and chelating agents. The intense reduction peaks at 550–600 °C are assigned to the molybdate in an octahedral site [4,14,44,45]. Previous results revealed that the formation of molybdate in the octahedral site was salutary for HDS reactions [4,42]. Therefore, the catalytic results confirm that the incorporations of proper amounts of nickel in the ordered mesoporous NiMo-$Al_2O_3$ catalysts contribute to the transformations of molybdate from the tetrahedral to the octahedral site, thus leading a high activity. Our present research reveals that when the *R* value is higher than 0.5 (as for the 10.0NiMoAl, 12.5NiMoAl, and 15.0NiMoAl catalysts), apparent changes of molybdate from the tetrahedral to the octahedral site together with relative TPR peak intensity simultaneously occur. On the other hand, when the contents of NiO further increased to 12.5 and 15.0 wt.% in the synthesis procedure, a decrease in the HDS activity is observed (Tables 3, 4, and Fig. 10), which might be attributed to the dispersions of active components. As the HRTEM micrographs (Figs. 5 and 6) and statistic analysis (Table 2) show, the average slab lengths of the $MoS_2$ nanoparticles on the 10.0NiMoAl and 15.0NiMoAl catalysts are 2.7 and 4.1 nm, respectively, and a higher stacking number of the $MoS_2$ nanoparticles is also confirmed on the 15.0NiMoAl catalyst than 10.0NiMoAl catalyst (2.1 v.s. 1.5). These factors contribute to a better dispersion of the $MoS_2$ nanoparticles on the 10.0NiMoAl catalyst ($f_{Mo}$ = 0.44) than on the 15.0NiMoAl catalyst ($f_{Mo}$ = 0.29). Therefore, the more agglomerated $MoS_2$ nanoparticles on the 15.0NiMoAl catalyst leads to a lower HDS activity towards DBT than on the 10.0NiMoAl catalyst. On the other hand, Tables 3 and 4 reveal that all the ordered mesoporous NiMo-$Al_2O_3$ catalysts have high HDS activities than the NiMo/meso-$Al_2O_3$ and NiMo/γ-$Al_2O_3$ catalysts, which are attributed to the better dispersion of active components by this EISA method and short-range ordered mesoporous structure. This is in accordance with the results reported by Soni et al. [12], and they found that compared to NiMo/γ-$Al_2O_3$ and NiMo/SBA-15 (a 2-D mesoporous support) catalysts, NiMo/KIT-6 (a 3-D mesoporous support) catalyst has a higher HDS activity due to the better dispersion of active components and faster diffusion of reactants and products [12].

In summary, the ordered mesoporous NiMo-$Al_2O_3$ catalyst, which was easily synthesized by a facile one-pot EISA method, showed high activities towards DBT. After further optimizing of some important factors, including Ni/Mo/Al ratios, calcination processes, and activation methods, we suppose that these ordered mesoporous NiMo-$Al_2O_3$ catalysts provide new alternatives for industrial applications.

## 4. Conclusions

A series of ordered mesoporous NiMo-$Al_2O_3$ catalysts were synthesized by an improved solvent evaporation-induced self-assembly (EISA) method by using P123 as surfactant and anhydrous ethanol as solvent. Calcination of the as-synthesized NiMo-$Al_2O_3$ precursors at 500 °C completely removed the surfactant and solvent, leading to the formation of hexagonally ordered mesoporous catalysts with a space group of *p6mm*. Incorporations of active components (NiO and $MoO_3$) in the synthesis procedure maintained the ordered mesoporous structure, and the active components were homogeneously distributed into the channels of alumina. Various contents of incorporated NiO in the synthesis procedure not only affected the centered temperatures of the NiMo-$Al_2O_3$ catalysts, but also changed their relative peak intensities. Catalytic results reveal that the ordered mesoporous NiMo-$Al_2O_3$ catalysts showed high activities towards DBT, and that BP occupied more than 85% of the whole product, indicating that DDS was the predominant way. Among these catalysts the 10.0NiMoAl catalyst, which had a Ni/Mo molar ratio of 1:1 (*R* = 0.5), showed a higher activity towards DBT than the other NiMo-$Al_2O_3$ catalysts, due to the formation of molybdate in octahedral site and high dispersion of $MoS_2$ nanoparticles. The highly-active ordered mesoporous NiMo-$Al_2O_3$ catalysts provide an alternative for industrial HDS process.

## Acknowledgements

The authors are highly appreciated for the kind help from Dr. Wei Wang from East China University of Science and Technology (ECUST) with the SEM experiments. Fruitful discussions with Dr. Peng Peng from China University of Petroleum (East China) are also appreciated. This work was financially supported by the National Natural Science Fund of China (Grants nos. U1162203 and 21106185) and the Fundamental Research Funds for the Central

Universities (grant nos. 14CX06032A and 14CX02059A). Financial support from PetroChina Corporation Limited is also greatly appreciated.

## Appendix A. Supplementary data

Supplementary data associated with this article can be found, in the online version, at http://dx.doi.org/10.1016/j.apcatb.2016.06.004.

## References

[1] Y. Sun, R. Prins, Angew. Chem. Int. Edit. 47 (2008) 8478–8481.
[2] W. Fu, L. Zhang, T. Tang, Q. Ke, S. Wang, J. Hu, G. Fang, J. Li, F.S. Xiao, J. Am. Chem. Soc. 133 (2011) 15346–15349.
[3] D. Valencia, T. Klimova, Appl. Catal. B: Environ. 129 (2013) 137–145.
[4] H. Liu, C. Liu, C. Yin, Y. Chai, Y. Li, D. Liu, B. Liu, X. Li, Y. Wang, X. Li, Appl. Catal. B: Environ. 174–175 (2015) 264–276.
[5] F.L. Plantenga, R. Cerfontain, S. Eijsbouts, F. van Houtert, G.H. Anderson, S. Miseo, S. Soled, K. Riley, K. Fujita, Y. Inoue, Sci. Technol. Catal. 89 (2002) 407–410.
[6] R.R. Chianelli, G. Berhault, B. Torres, Catal. Today 147 (2009) 275–286.
[7] S.L. Amaya, G. Alonso-Núñez, T.A. Zepeda, S. Fuentes, A. Echavarría, Appl. Catal. B: Environ. 148–149 (2014) 221–230.
[8] H. Liu, C. Yin, H. Li, B. Liu, X. Li, Y. Chai, Y. Li, C. Liu, Fuel 129 (2014) 138–146.
[9] A.S. Walton, J.V. Lauritsen, H. Topsøe, F. Besenbacher, J. Catal. 308 (2013) 306–318.
[10] M. Breysse, P. Afanasiev, C. Geantet, M. Vrinat, Catal. Today 86 (2003) 5–16.
[11] G.M. Dhar, B.N. Srinivas, M.S. Rana, M. Kumar, S.K. Maity, Catal. Today 86 (2003) 45–60.
[12] K. Soni, B.S. Rana, A.K. Sinha, A. Bhaumik, M. Nandi, M. Kumar, G.M. Dhar, Appl. Catal. B: Environ. 90 (2009) 55–63.
[13] W. Fu, L. Zhang, D. Wu, M. Xiang, Q. Zhuo, K. Huang, Z. Tao, T. Tang, J. Catal. 330 (2015) 423–433.
[14] S. Garg, K. Soni, T. Ajeeth Prabhu, K.S. Rama Rao, G. Murali Dhar, Catal. Today 261 (2016) 128–136.
[15] C. Boissiere, D. Grosso, A. Chaumonnot, L. Nicole, C. Sanchez, Adv. Mater. 23 (2011) 599–623.
[16] J. Čejka, Appl. Catal. A: Gen. 254 (2003) 327–338.
[17] N. Wang, K. Shen, L. Huang, X. Yu, W. Qian, W. Chu, ACS Catal. 3 (2013) 1638–1651.
[18] Q. Yuan, A.X. Yin, C. Luo, L.D. Sun, Y.W. Zhang, W.T. Duan, H.C. Liu, C.H. Yan, J. Am. Chem. Soc. 130 (2008) 3465–3472.
[19] Q. Liu, J. Gao, F. Gu, X. Lu, Y. Liu, H. Li, Z. Zhong, B. Liu, G. Xu, F. Su, J. Catal. 326 (2015) 127–138.
[20] L. Xu, H. Song, L. Chou, ACS Catal. 2 (2012) 1331–1342.
[21] J. Horiguchi, Y. Kobayashi, S. Kobayashi, Y. Yamazaki, K. Omata, D. Nagao, M. Konno, M. Yamada, Appl. Catal. A: Gen. 392 (2011) 86–92.
[22] S.M. Morris, P.F. Fulvio, M. Jaroniec, J. Am. Chem. Soc. 130 (2008) 15210–15216.
[23] Q. Wu, F. Zhang, J. Yang, Q. Li, B. Tu, D. Zhao, Microporous Mesoporous Mater. 143 (2011) 406–412.
[24] D. Genuit, P. Afanasiev, M. Vrinat, J. Catal. 235 (2005) 302–317.
[25] H. Wang, R. Prins, J. Catal. 264 (2009) 31–43.
[26] H. Liu, C. Yin, B. Liu, X. Li, Y. Li, Y. Chai, C. Liu, Energy Fuel 28 (2014) 2429–2436.
[27] K.S.W. Sing, D.H. Everett, R.A.W. Haul, L. Moscou, R.A. Pierotti, J. Rouquérol, T. Siemieniewska, Pure Appl. Chem. 57 (1985) 603–619.
[28] J. Čejka, P.J. Kooyman, L. Veselá, J. Pérez-Pariente, A.B. Pinar, A. Zukal, J. Čejka, Phys. Chem. Chem. Phys. 3 (2001) 5076–5081.
[29] K. Niesz, P. Yang, G.A. Somorjai, Chem. Commun. 15 (2005) 1986–1987.
[30] O.Y. Gutiérrez, T. Klimova, J. Catal. 281 (2011) 50–62.
[31] F. Kleitz, W. Schmidt, F. Schüth, Microporous Mesoporous Mater. 65 (2003) 1–29.
[32] M.B. Yue, W.Q. Jiao, Y.M. Wang, M.Y. He, Microporous Mesoporous Mater. 132 (2010) 226–231.
[33] F. Bérubé, S. Kaliaguine, Microporous Mesoporous Mater. 115 (2008) 469–479.
[34] D.M. Ibrahim, Y.M. Abu-Ayana, Mater. Chem. Phys. 113 (2009) 579–586.
[35] Z. Zhu, H. Liu, H. Sun, D. Yang, Microporous Mesoporous Mater. 123 (2009) 39–44.
[36] K.M. Parida, A.C. Pradhan, J. Das, N. Sahu, Mater. Chem. Phys. 113 (2009) 244–248.
[37] P.R. Aravind, P. Mukundan, P. Krishna Pillai, K.G.K. Warrier, Microporous Mesoporous Mater. 96 (2006) 14–20.
[38] I. Eswaramoorthi, V. Sundaramurthy, N. Das, A.K. Dalai, J. Adjaye, Appl. Catal. A: Gen. 339 (2008) 187–195.
[39] A. Wang, Y. Wang, T. Kabe, Y. Chen, A. Ishihara, W. Qian, J. Catal. 199 (2001) 19–29.
[40] A. Wang, Y. Wang, T. Kabe, Y. Chen, A. Ishihara, W. Qian, P. Yao, J. Catal. 210 (2002) 319–327.
[41] J. Zhang, Z. Xin, X. Meng, Y. Lv, M. Tao, Fuel 116 (2014) 25–33.
[42] C.F. Linares, M. Fernández, Catal. Lett. 126 (2008) 341–345.
[43] E. Salehi, F.S. Azad, T. Harding, J. Abedi, Fuel Process. Technol. 92 (2011) 2203–2210.
[44] R. Nava, R.A. Ortega, G. Alonso, C. Ornelas, B. Pawelec, J.L.G. Fierro, Catal. Today 127 (2007) 70–84.
[45] J.L. Brito, A.L. Barbosa, A. Albornoz, F. Severino, J. Laine, Catal. Lett. 26 (1994) 329–337.
[46] M. Egorova, R. Prins, J. Catal. 225 (2004) 417–427.
[47] H. Wang, R. Prins, J. Catal. 258 (2008) 153–164.
[48] M. Egorova, R. Prins, J. Catal. 221 (2004) 11–19.
[49] E. Krebs, B. Silvi, P. Raybaud, Catal. Today 130 (2008) 160–169.
[50] D. Solis, T. Klimova, J. Ramíez, T. Cortez, Catal. Today 98 (2004) 99–108.
[51] E. Altamirano, J.A. de los Reyes, F. Murrieta, M. Vrinat, J. Catal. 235 (2005) 403–412.